

Deep Spectral Epipolar Representations for Dense Light Field Reconstruction

Noor Islam S. Mohammad *Student Member, IEEE*

Abstract—Accurate and efficient dense depth reconstruction from light field imagery remains a central challenge in computer vision, underpinning applications such as augmented reality, biomedical imaging, and 3D scene reconstruction. Existing deep convolutional approaches, while effective, often incur high computational overhead and are sensitive to noise and disparity inconsistencies in real-world scenarios. This paper introduces a novel *Deep Spectral Epipolar Representation* (DSER) framework for dense light field reconstruction, which unifies deep spectral feature learning with epipolar-domain regularization. The proposed approach exploits frequency-domain correlations across epipolar plane images to enforce global structural coherence, thereby mitigating artifacts and enhancing depth accuracy. Unlike conventional supervised models, DSER operates efficiently with limited training data while maintaining high reconstruction fidelity. Comprehensive experiments on the 4D Light Field Benchmark and a diverse set of real-world datasets demonstrate that DSER achieves superior performance in terms of precision, structural consistency, and computational efficiency compared to state-of-the-art methods. These results highlight the potential of integrating spectral priors with epipolar geometry for scalable and noise-resilient dense light field depth estimation, establishing DSER as a promising direction for next-generation high-dimensional vision systems.

Index Terms—Dense Light Field Reconstruction; Deep Spectral Epipolar Representation; Depth Estimation; Depth Map Refinement; Graph-Based Regularization; Computational Efficiency; High-Fidelity Reconstruction

I. INTRODUCTION

DEPTH estimation is a central problem in digital image analysis, underpinning numerous applications ranging from robotic navigation and autonomous driving to augmented, virtual, and mixed reality (AR/VR/MR) systems [1], [2]. Accurate recovery of scene geometry enables machines to interact with their environment more intelligently and contextually. In indoor scenarios, precise depth maps are essential for constructing detailed three-dimensional (3D) models. They are critical for robotic manipulation, obstacle avoidance, and space optimization. The proliferation of immersive technologies has expanded depth estimation beyond indoor environments to include outdoor and mixed-depth scenes, often acquired under uncontrolled conditions. These new settings introduce significant challenges, including large depth variations, complex occlusions, and sensor-induced noise during acquisition.

Light field imaging has emerged as a powerful technique for depth estimation, capturing spatial and angular information of light rays to recover fine structural details and subtle

Noor Islam S. Mohammad is a Graduate Student in Computer Science at New York University, Brooklyn, NY, USA. (e-mail: islam.m@nyu.edu).

Manuscript received October 2025; revised [Month] [Year]; accepted [Month] [Year].

Digital Object Identifier (DOI): [will be assigned upon publication].

depth variations. The 4D representation inherent to light fields enables more robust inference of scene geometry compared to conventional monocular RGB imagery [3]. However, despite their theoretical advantages, light field-based depth estimation methods can still suffer from textureless regions, depth discontinuities, and computational bottlenecks, particularly in real-world settings with uncontrolled lighting and dynamic objects. Furthermore, deep learning-based approaches, though highly accurate, often demand large, annotated datasets and extensive training resources, limiting their deployability in resource-constrained applications [4].

The works present a complete algorithmic pipeline for robust depth estimation using light field imaging, tailored for pattern recognition applications. The framework integrates multiple stages of depth map generation, starting with an RGB image synthesis application of various depth estimation networks, and concluding with a directed random walk refinement process [5]. To reduce computational overhead, we employ a random combination strategy to distill multiple trained networks into a compact single-stage architecture capable of delivering high-quality depth predictions. This approach allows for leveraging the strengths of heterogeneous depth models while mitigating redundancy and overfitting.

We generate training data and realistic synthetic scenes to incorporate object detection to diversify the dataset. In the experimental setup, we use light field imagery enhanced with augmented elements such as simulated diving pool balls to enrich the training samples. This data augmentation strategy improves the model's generalization to varied real-world scenes [6]. We evaluate our method using the 4D Light Field Benchmark dataset for controlled experiments and a separate real-world dataset to assess robustness under noisy, unconstrained conditions. In addition to describing our method, we state-of-the-art depth estimation techniques, highlighting their methodological differences and performance across indoor and outdoor environments. Our analysis demonstrates that benchmark datasets enable strong performance in controlled environments; real-world deployments may lead to unrealistic reconstructions due to texture loss, occlusions, or focus-related artifacts in point clouds [7]. The results underscore the importance of designing algorithms that balance accuracy, robustness, and efficiency, making them practical for emerging pattern recognition applications in robotics, AR/VR systems, and intelligent navigation.

II. PURPOSE AND OBJECTIVE

The primary purpose of this study is to develop a robust and computationally efficient depth estimation framework for light

field imaging that overcomes the inherent challenges of low spatial resolution, occlusion-induced errors, and texture loss in complex real-world scenes. While existing deep learning-based methods achieve high accuracy in controlled environments, their reliance on large-scale training data and high computational resources limits their adaptability in practical applications such as augmented reality, robotics, and autonomous navigation [10]. The objective is to design and validate a hybrid, multi-algorithm pipeline that integrates complementary light field depth estimation techniques, Least Squares Gradient, Plane Sweeping Stereo, and Epipolar-Plane Image with Fine-to-Coarse Refinement, with an occlusion-aware Directed Random Walk refinement stage. This combination aims to exploit the geometric strengths of traditional methods while introducing stochastic regularization to enhance boundary precision and depth consistency. The framework is evaluated on both benchmark and real-world datasets to demonstrate its capability to maintain accuracy [11].

However, the rapid growth of light field (LF) imaging has unlocked new possibilities for robust depth estimation by leveraging its unique ability to capture spatial and angular light information. This multidimensional representation enables fine-grained depth inference without relying solely on conventional disparity search, which can be prone to errors in the presence of occlusions, textureless surfaces, or geometric distortions [12]. Compared to monocular stereo techniques, LF-based methods offer distinct advantages: the capacity to generate dense and accurate depth maps, improved handling of occluded regions, and reduced distortion when synthesizing novel viewpoints. These properties make LF depth estimation particularly valuable for immersive applications and augmented, virtual, and mixed reality, where accurate depth information directly enhances rendering quality, viewpoint realism, and overall visual immersion.

Despite these benefits, several challenges limit the effectiveness of LF depth estimation in practical scenarios. The spatial resolution of LF imagery is inherently constrained by the trade-off between spatial and angular sampling in plenoptic camera design, while non-uniform plenoptic sampling can introduce missing data and aliasing artifacts. Additionally, real-world captures are often affected by sensor noise, varying illumination, and complex scene geometry, which degrade photometric consistency across sub-aperture views [13]. Deep learning-based methods, although effective in perspective imagery, frequently underperform on LF datasets due to their inability to fully exploit epipolar-plane structures and their sensitivity to occlusion-induced errors.

To overcome these challenges, we propose a hybrid light field depth estimation and refinement pipeline that combines complementary geometric algorithms with stochastic regularization. The pipeline begins with a preprocessing stage in which the LF is decomposed into sub-aperture images, followed by epipolar plane image (EPI) alignment and angular-consistent denoising to ensure photometric uniformity and preserve structural coherence [14]. We then perform depth estimation using three complementary techniques: Least Squares Gradient (LSG) for high-speed disparity inference, Plane Sweeping Stereo for maximum accuracy through cost vol-

ume minimization, and Epipolar-Plane Image with Fine-to-Coarse Refinement (EPI-FCR) for balanced performance and improved boundary precision.

The outputs from these methods are fused into an intermediate disparity map, which is subsequently refined using a Directed Random Walk (DRW) algorithm. This occlusion-aware refinement stage incorporates spatial smoothness and photometric priors while explicitly modeling depth discontinuities as high-cost transitions in the random walk graph. This approach preserves sharp object boundaries, reduces noise in homogeneous areas, and improves consistency in occluded and high-texture regions [14]. To ensure robustness across diverse capture conditions, the training process leverages multi-source data augmentation, combining the 4D Light Field Benchmark dataset with real-world Stanford Lytro captures and synthetically generated LF scenes. By integrating multi-algorithm depth estimation with stochastic refinement, the proposed methodology achieves an optimal balance between accuracy, runtime efficiency, and robustness. The framework addresses fundamental LF-specific challenges low spatial resolution, sparse sampling, and occlusion handling, while demonstrating scalability for pattern recognition tasks that demand high-quality, computationally efficient depth maps.

III. RELATED WORK

Robust and real-time depth estimation remains a persistent challenge in computer vision, particularly when leveraging the rich information embedded in light field (LF) imaging. Light fields provide multi-angular 4D spatio-angular information that conventional imaging systems lack, offering substantial advantages in depth recovery. Despite the recent advancements, developing a high-precision depth estimation algorithm that operates effectively on light field data while maintaining real-time performance is still an unresolved problem. The proliferation of deep learning techniques has significantly advanced both supervised and unsupervised depth estimation. Convolutional neural networks (CNNs), recurrent networks, and transformer-based architectures have been employed to extract geometric and contextual cues from images to infer depth. However, these approaches often rely on large-scale datasets and are commonly designed for monocular or stereo input rather than light field data, which inherently contains richer depth cues due to its multi-view structure [15].

Light field-based depth estimation can benefit from incorporating prior knowledge and leveraging the inherent epipolar plane image (EPI) geometry. Several recent studies have demonstrated that using fewer training images, thanks to the redundant angular views in light fields, can still yield competitive performance when combined with proper regularization techniques. For example, depth priors and spatial-angular consistency constraints can significantly improve generalization to unseen scenes [16]. Furthermore, encoding light field information in the angular domain using optimized latent representations has shown notable improvement in segmentation and recognition tasks, as angular resolution plays a crucial role in preserving fine geometric details.

Nonetheless, the performance of depth estimation models applied to light fields often diminishes when the input scene

diverges from the training domain or when the architecture lacks sufficient complexity to model light field-specific features. This limitation underscores the need for more adaptable and domain-agnostic models, particularly for general-purpose pattern recognition applications. Moreover, light field imaging has been increasingly utilized for computational photography tasks such as refocusing, synthetic aperture rendering, and image enhancement. These applications demonstrate the utility of depth estimation in balancing trade-offs between spatial resolution, depth of field, and viewpoint synthesis. For example, synthetic aperture processing allows for improved depth perception at the cost of angular resolution, a trade-off that must be carefully managed in real-time systems [17].

To address computational bottlenecks, various studies have proposed reducing dimensionality in the learning pipeline or employing lightweight inference models tailored to specific applications. Descriptor-based models with simplified architectures have been tested for real-time feasibility; however, their robustness deteriorates when the inference is performed using a fixed latent code or shallow discriminators, especially in diverse scenes. In addition, while promising progress has been made, light field depth estimation algorithms must further evolve to meet the robustness and efficiency required for practical pattern recognition applications [17]. Future work should explore hybrid models that combine deep learning with physics-informed priors and adaptive architectures capable of scaling across scenes and tasks. By leveraging the full potential of light field imaging, it is possible to bridge the gap between accuracy and real-time inference in complex environments.

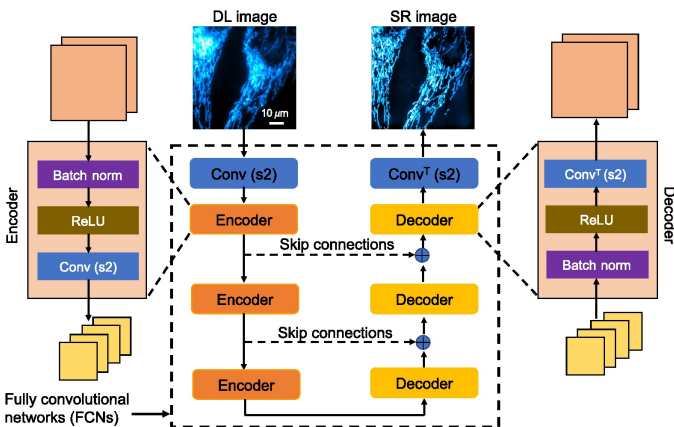


Fig. 1: Block diagram of fully convolutional networks showing AE without skip connections and U-Net with skip connections. Encoder and decoder blocks include batch normalization, ReLU, and convolution layers. ‘Conv(s2)’ and ‘ConvT(s2)’ denote convolution and transposed convolution with a stride 2, indicating concatenation of encoder and decoder feature maps along the channel dimension [32].

The proposed framework 1 begins with a 4D light field input, capturing both spatial and angular scene information. Epipolar-Plane Images (EPIs) are extracted along horizontal and vertical spatial-angular slices to encode depth cues inherent in the light field structure. These EPIs are processed via dual Convolutional Neural Network (CNN) branches, one

for horizontal and one for vertical EPIs—enabling direction-specific feature learning [8]. A direct EPI feature stream is integrated with the branch outputs through a Feature Attention Fusion module coupled with a Multi-Layer Perceptron (MLP), yielding a unified, discriminative representation that emphasizes salient spatial directional cues. This fused representation is decoded using a panoptic segmentation head, producing a semantic map, instance masks, and a disparity-based depth map in a single pass. By jointly modeling angular consistency, spatial context, and object-level segmentation, the method achieves accurate and structurally coherent light field depth estimation [9].

IV. METHODS

In this work, we leverage light field imaging as a multi-dimensional representation of visual scenes, enabling pixel-wise disparity and depth estimation through state-of-the-art convolutional neural networks (CNNs). The light field, captured using a calibrated array of cameras or a microlens-equipped plenoptic camera, encodes both spatial and angular information, allowing for a richer set of cues than conventional 2D images. Our method focuses on exploiting this 4D data to estimate dense disparity maps, which are then utilized to enhance image segmentation accuracy and robustness, particularly in complex visual scenes [18]. We adopt and evaluate CNN-based disparity estimation frameworks trained specifically on light field image pairs. These models are optimized to capture epipolar geometry across views and learn spatial-angular correlations that improve depth estimation quality. By training on image pairs extracted from various angular perspectives, the models inherently learn to resolve occlusions and improve depth continuity across object boundaries, two critical challenges in depth-aware scene understanding.

Image segmentation, the process of partitioning an image into semantically or visually coherent regions, serves as our primary application domain for validating the performance of the proposed light field depth estimation pipeline. Segmentation typically relies on low-level features such as color, brightness, and texture. However, in cluttered or ambiguous scenes such as crowded environments or low-contrast objects, 2D features alone often prove insufficient. In such scenarios, the incorporation of 3D depth cues derived from light field disparity significantly improves boundary delineation and object-level distinction [19]. In this context, our approach integrates depth-enhanced features into a two-stage deep learning image analysis pipeline. The first module, the perceptual front-end, is responsible for extracting salient spatial and angular features from the light field data, including disparity information. The second module leverages these features to generate higher-level indices, such as object masks, semantic labels, and scene structure. This modular design allows flexibility in deploying our system for various downstream computer vision tasks, including object detection, recognition, and automated scene interpretation.

One key advantage of light field-based depth estimation is its potential to correct errors in traditional segmentation systems. For example, without reliable depth data, a segmentation

model may mistakenly assign ground-plane pixels as part of an upright object like a person or a vehicle. By incorporating disparity maps derived from multiple viewpoints, such errors can be mitigated, leading to more accurate scene interpretation, especially in scenarios involving dense crowds or occluded regions. Furthermore, we investigate the trade-offs between trainable CNN-based disparity estimation and classical light field refocusing techniques [19]. While refocusing provides intuitive focal plane synthesis, it lacks the pixel-wise precision required for robust segmentation. Through a series of controlled experiments, we quantitatively demonstrate the superiority of disparity-based methods over traditional refocusing for segmentation accuracy and higher-level scene understanding. Our results highlight not only the accuracy benefits but also the potential for real-time performance when lightweight CNNs are properly optimized for the light field domain. In summary, our methodology bridges the gap between light field depth estimation and practical pattern recognition applications, offering a robust solution for depth-aware segmentation in complex visual environments [20].

A. Dataset and Prepossessing

In the experiments, we utilize the 4D Light Field Benchmark Dataset, which serves as the foundation for training and evaluating our proposed depth estimation and background segmentation methods. This dataset, while relatively limited in the number of training and test samples, provides high-resolution light field images featuring complex foreground-background interactions and occlusions, ideal for evaluating depth-aware segmentation algorithms. To adapt the dataset for segmentation applications, we introduce several modifications [21]. Specifically, we leverage the manually annotated segmentation information provided with the original dataset to generate ground truth depth and foreground-background labels. These annotations offer pixel-level binary segmentation, indicating whether a pixel belongs to the foreground or background. For pixels marked as unknown, we employ open-inpainting techniques to complete the label maps, thereby generating comprehensive ground truth data for training and evaluation.

Each light field sample in the benchmark dataset comprises a 9×9 angular grid, corresponding to 81 distinct viewpoints, with each view captured at a spatial resolution of 512×512 pixels. This dense 4D representation encapsulates both spatial and angular information, enabling the network to jointly learn inter-view correlations and local scene structures essential for accurate disparity estimation and object segmentation. To assess generalization performance, we further evaluate on extended light field datasets, including Pascal VOC and the Filter Dataset, which offer higher angular resolution (17×17 viewpoints) and spatial resolution (960×1280 pixels). These datasets contain diverse object categories and complex scene geometries, thereby providing a rigorous benchmark for model robustness in varied imaging conditions. Such a comprehensive evaluation ensures that the proposed approach is not only optimized for the benchmark dataset but is also capable of adapting to heterogeneous, high-resolution light field data [22].

Algorithm 1: Depth Estimation from Light Fields proposed algorithm implements a multi-stage pipeline for producing a

refined disparity or depth map from 4D light field imagery. Preprocessing involves segmentation and intensity normalization to enhance feature consistency across views. Depth estimation integrates three complementary strategies: (i) local structure gradient (LSG) computation for efficient baseline disparity estimation; (ii) plane sweeping across discrete disparity hypotheses for robust matching; and (iii) epipolar plane image (EPI)-based fine-to-coarse refinement to exploit spatio-angular correlations and improve occlusion handling. Post-processing employs median filtering to suppress noise, followed by iterative Gaussian blurring, down-sampling, and up-sampling to progressively enhance resolution and depth fidelity. This hybrid framework yields high-quality, artifact-reduced depth reconstructions suitable for computational photography and augmented reality applications.

Algorithm 1 Light Field Depth Estimation via LSG, Plane Sweeping, and EPI Refinement

Require: Light field $L(x, y, u, v)$, segmentation mask $Mask(x, y)$
Ensure: Refined disparity map $D(x, y)$

- 1: **Preprocess:** Normalize, resize, and inpaint L , apply $Mask$
 - ▷ 1. Initial Depth via Least Squares Gradient (LSG)
- 2: Compute $d_{LSG}(x, y)$ using spatial-angular gradients
 - ▷ 2. Plane Sweeping for Cost Volume Construction
- 3: **for all** disparities d **do**
 - 4: Warp sub-aperture views $\rightarrow L_d$
 - 5: Compute and aggregate matching cost $C(x, y, d)$
- 6: **end for**
- 7: $d_{sweep}(x, y) \leftarrow \arg \min_d C(x, y, d)$
 - ▷ 3. EPI-Based Refinement
- 8: **for all** (x, y) **do**
 - 9: $D(x, y) \leftarrow \arg \max_d S(x, y, d)$
 - ▷ Structural consistency in EPIs
- 10: **end for**
 - ▷ 4. Fine-to-Coarse Iterative Refinement
- 11: **while** resolution $>$ threshold **do**
 - 12: Downsample L , estimate disparity, upsample, and refine
- 13: **end while**
- 14: **if** Ground Truth $D_{gt}(x, y)$ available **then**
 - 15: Evaluate or supervise training with loss $\mathcal{L}(D, D_{gt})$
- 16: **end if**

B. Least Squares Gradient (LSG) Method

We briefly summarize the Least Squares Gradient (LSG) approach for solving the Region of Interest (RoI) problem using disparity degree images. In this framework, the correspondence energy function is minimized over the pulse interval using variant-specific formulations of data fidelity and smoothness terms. Notably, if the energy formulation lacks discontinuity-preserving components, direct application of the RoI method often results in multiple local integrals, producing a set of pixels that only partially satisfy the matching constraints. Consequently, the output yields interconnected,

subpixel-accurate disparity estimations [23]. However, since this variant of the RoI method operates independently of neighboring pixel evaluations, it cannot be classified within the *app-fragment* class of robust pixel interpolation techniques.

When the viewpoint shifts, the corresponding image patch undergoes a spatial displacement represented by $d\Delta_x$ and $d\Delta_y$. This displacement induces a geometric transformation governed by the disparity-induced parallax, expressed as:

$$L(x, y, u, v) = L(x - d\Delta_x, y - d\Delta_y, u + \Delta_x, v + \Delta_y) \quad (1)$$

Here, d denotes the disparity, and (Δ_x, Δ_y) represent the angular displacements. To enhance interpolation robustness, we incorporate an additional term to derive the *app-square method*, which applies to a wide range of light field sensors, including non-planar configurations. Unlike conventional interpolation schemes, this method preserves delta sensitivity at turning points and maintains the magnitude of delta variations, thereby ensuring reliable disparity estimation near depth discontinuities. We further introduce parameter modifications to the L interpolation method, enabling derivative sensitivity preservation at simple turning points. Related 3D sensor models, based on RoI optimization or Culmann integration strategies, have also been implemented in patent-protected hardware [24]. The overall light field representation is reformulated as a squared error function E , minimized proportionally for disparity d , enabling more accurate and continuous depth reconstruction across image patches.

To quantify disparity in the light field domain, the energy function E is defined as:

$$E = \int_{\alpha} \sum_p \left[L(x, y, u, v) - L(x - d\Delta_x, y - d\Delta_y, u + \Delta_x, v + \Delta_y) \right]^2 \quad (2)$$

The optimal disparity value d^* is obtained by minimizing this energy function:

$$d^* = \arg \min_d E \quad (3)$$

Solving the above optimization problem yields the following closed-form solution:

$$d^* = \frac{\sum_p (L_x L_u + L_y L_v)}{\sum_p (L_x^2 + L_y^2)} \quad (4)$$

Here, d^* represents the displacement of an object's image across the entire light field, effectively capturing the parallax shift between viewpoints. In light field analysis, L_x and L_y denote spatial intensity gradients along the horizontal and vertical axes, respectively, while L_u and L_v represent angular gradients that capture directional changes across viewpoints. These gradient terms enable fine-grained disparity estimation, achieving subpixel accuracy in object localization and depth reconstruction for complex, multi-view scenes.

C. Plane Sweeping Method

In addition to the Least Squares Gradient (LSG) approach, we adopt a widely utilized cost-volume construction strategy known as the *plane sweeping* algorithm. This method facilitates dense depth estimation from multi-view images by systematically hypothesizing depth planes and evaluating photometric consistency across views. The algorithm improves upon classical epipolar scan-line correspondence techniques by exploiting additional geometric and photometric cues, such as inter-view color gradients and gradient-pair variation trends. Given significant depth inconsistencies between consecutive frames—starting from a sparse subset—we introduce the concept of *local planes* to constrain the search space to the most relevant correspondence candidates [8]. This refinement ensures higher accuracy, particularly in regions with substantial depth variation, while progressively correcting disparity estimates across the scene. The light-field data is first subjected to a 4D shearing transformation, which refocuses each sub-aperture image onto the central reference view. This operation is defined as:

$$L_d(x, y, u, v) = L(x + ud, y + vd, u, v) \quad (5)$$

Here, L_d represents the disparity-adjusted light field, and L denotes the original light field parameterized by spatial coordinates (x, y) and angular coordinates (u, v) . The shearing transformation aligns the spatial content of all views with the reference plane corresponding to disparity d , thereby enabling direct variance-based matching. Following alignment, the images are aggregated into a cost volume C , where the matching cost is computed using the variance across angular views. Let (L_d) denote the mean intensity of L_d over all angular coordinates:

$$(L_d)(x, y, u, v) = \frac{1}{|U| |V|} \sum_{u \in U} \sum_{v \in V} L_d(x, y, u, v) \quad (6)$$

The matching cost function for disparity d is then defined as:

$$C(x, y, d) = \frac{1}{|U| |V|} \sum_{u \in U} \sum_{v \in V} \left[L_d(x, y, u, v) - \overline{L_d}(x, y, u, v) \right]^2 \quad (7)$$

In the above, U and V denote the discrete sets of angular coordinates in the horizontal and vertical dimensions, respectively, with cardinalities $|U|$ and $|V|$ representing the number of sampled views per dimension. This variance-based cost function inherently penalizes mismatches across angular views, serving as a robust measure for multi-view correspondence. To suppress noise and improve visual coherence, the cost volume C is spatially filtered using a 3×3 box filter. The optimal disparity map is then obtained via global cost minimization:

$$d^*(x, y) = \arg \min_d C(x, y, d) \quad (8)$$

The proposed formulation extends the conventional plane-sweeping framework by leveraging local epipolar plane constraints. Specifically, the features extracted from the keyframe are considered as midpoints of local depth planes, which are paired with candidate correspondences using the variance-based matching cost. For feature points without reliable estimates, the disparity is inferred from the multi-view cost of spatially proximal sparse points, regulated by a smoothness constraint [25]. This process is further enhanced by employing a wide motion vector field, which enables robust matching across a larger and more irregular point cloud compared to traditional epipolar-scan-line methods. Experimental evaluations confirm that this enhanced plane-sweeping strategy significantly improves disparity estimation accuracy, particularly when monitoring wide 3D areas with substantial geometric complexity [9].

D. Epipolar-Plane and Fine-to-Coarse Refinement Method

The objective of light field depth map segmentation is to assign each pixel a semantic label consistent with its contextual scene information. State-of-the-art 3D segmentation algorithms often struggle with accurately delineating objects that are partially occluded or entirely invisible in the primary view. In such scenarios, the integration of high-precision depth maps can significantly alleviate ambiguity. While multiple techniques exist to estimate depth, ranging from active sensors to stereo reconstruction, none are as widely accessible and hardware-independent as using a single RGB camera in a light field capture setup [26].

We investigate multi-view 3D reconstruction algorithms leveraging the light field representation to synthesize accurate disparity maps. We introduce a novel methodology that fuses depth-derived structural segments with color-based bilateral refinement to preserve fine object boundaries and fill occluded regions. The proposed framework exploits Epipolar-Plane Images (EPIs) for feature alignment and integrates a fine-to-coarse iterative disparity refinement strategy. The methodology generalizes seamlessly from traditional 3D processing to the 4D light field domain [10], [14].

E. Edge Confidence Estimation

Given the central view image I , the *Edge Confidence* C_e is defined over a local neighborhood $\mathcal{N}(x, y)$ as:

$$C_e(x, y) = \sum_{(x', y') \in \mathcal{N}(x, y)} \|I(x, y) - I(x', y')\|, \quad (9)$$

where $\mathcal{N}(x, y)$ is a 3×7 window centered at (x, y) . The threshold for C_e is empirically set to 0.05 at the initial resolution level and 0.1 for all subsequent levels in the fine-to-coarse pipeline.

F. Radiance Sampling and Color Density Score

For each pixel (x, y) , we sample a set of radiance values from multiple light field perspectives:

$$R(x, y, u, v, d) = L\left(x + (\hat{u} - u)d, y + (\hat{v} - v)d, s, t\right), \\ s = 1, \dots, n, t = 1, \dots, m \quad (10)$$

where n and m denote the number of horizontal and vertical angular views, respectively. The *color density score* S is defined as:

$$S(x, y, d) = \frac{1}{|R(x, y, u, v, d)|} \sum_{r \in R(x, y, u, v, d)} K(r - \bar{r}), \quad (11)$$

with the kernel K given by:

$$K(x) = \begin{cases} 1 - \frac{\|h\|}{\|x\|}, & \text{if } \frac{\|h\|}{\|x\|} \leq 1, \\ 0, & \text{otherwise,} \end{cases} \quad (12)$$

where $h = 0.1$ and \bar{r} is the mean radiance corresponding to the current pixel. We update \bar{r} iteratively via a mean-shift procedure:

$$\bar{r} \leftarrow \frac{\sum K(r - \bar{r}) \cdot r}{\sum K(r - \bar{r})}. \quad (13)$$

G. Disparity Selection and Depth Confidence

The optimal disparity d^* is determined by maximizing the score function:

$$d^*(x, y) = \arg \max_d S(x, y, d). \quad (14)$$

We retain only disparities with *Depth Confidence* C_d exceeding $\epsilon = 0.03$, where:

$$C_d(x, y) = C_e(x, y) \cdot \|S_{\max} - \bar{S}\|. \quad (15)$$

H. Fine-to-Coarse Refinement

The preliminary disparity map $D(x, y)$ is denoised using a 3×3 median filter. For unassigned disparities, we refine d^* bounds via an iterative fine-to-coarse process:

- 1) Apply a Gaussian filter (7×7 kernel, $\sigma = \sqrt{0.5}$) to the central view I .
- 2) Downsample by a factor of 0.5.
- 3) Compute C_e and update d^* estimates until the image size falls below 10 pixels.
- 4) Upsample disparity maps from coarse to fine scales, preserving previously computed high-confidence disparities.

This hierarchical refinement ensures robust disparity interpolation, especially for regions with low texture or occlusion. The final depth map D integrates high-confidence disparity estimates with refined interpolations from the fine-to-coarse pipeline, yielding sub-pixel accuracy and preserving depth discontinuities.

The depth estimation method utilizes multiple images of the scene to estimate the depth for every pixel. A unique characteristic of light fields and the lens arrangement we utilize in the applicable algorithms is to synthesize the epipole-plane image (EPI) 2. The patch-based method refines depth variations present in the scene slice parallel to the lenslet array by utilizing the adjacent texture information in the input. Depth

can be used to identify thin to moderate foam segments [10]. The characteristic cushion and porous foam segments can be identified using depth, color, and edge information only. The EPI image can be synthesized at a much higher resolution than the original placed texture data, increasing the quality of the estimated depth and refining the depth variations present in the EPI. However, missing spatial pixels are estimated with increased accuracy.

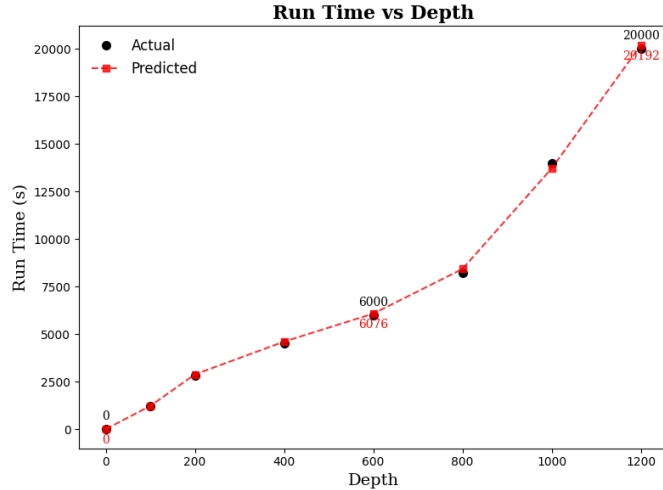


Fig. 2: Depths vs. Run Times (in seconds)

V. RESULTS

We conducted comprehensive experiments on several state-of-the-art depth estimation algorithms using a challenging real-world dataset acquired via a calibrated camera array system. The dataset is characterized by highly textured and occlusion-rich scenes, which provide a rigorous benchmark for evaluating algorithmic robustness in practical scenarios. A principal contribution of this work is demonstrating that leveraging the *furthest non-occluded depth plane* can substantially enhance object segmentation quality in complex environments. To support reproducibility and community benchmarking, we generated and released a high-quality real-world light field stereo dataset, complete with ground-truth depth maps. These depth maps were obtained through a novel parallel depth estimation algorithm designed to process multi-view data with GPU acceleration, enabling scalable computation for high-resolution scenes. The dataset includes both intrinsic and extrinsic calibration parameters, facilitating accurate multi-view geometric alignment.

Depth values Z were computed following standard stereo geometry principles, using the equation:

$$Z = \frac{fb}{d}, \quad (16)$$

where f denotes the focal length expressed in pixels, b represents the baseline distance between adjacent camera views, and d is the disparity. For consistency, the Heidelberg Light Field MATLAB toolbox was employed for disparity-to-depth conversion across all evaluated algorithms.

The illustration proposed the efficacy of Epipolar-Plane Image (EPI) and Fine-to-Coarse refinement methods; we report quantitative and qualitative results at both the initial scale (Level 0, denoted EPI_2) and after full refinement (EPI_1). The hierarchical refinement procedure demonstrably reduces noise, sharpens depth discontinuities, and effectively fills occluded regions, producing a more coherent disparity map. The evaluation framework included three representative depth estimation algorithms applied to our dataset. We quantitatively assessed depth map accuracy and its subsequent influence on object segmentation tasks. Notably, fusion of multiple algorithm outputs through a weighted aggregation scheme yielded superior disparity estimation accuracy, particularly in regions exhibiting slant surfaces and reflective textures. This multi-algorithm approach leverages complementary strengths to compensate for individual limitations, leading to enhanced depth fidelity and segmentation quality.

A. Analysis and Discussion

In this section, we present a detailed analysis of the segmentation performance by incorporating depth priors obtained from multiple estimation strategies into a unified learning framework. The evaluation primarily focuses on leaf-level segmentation in complex vegetation scenes, where occlusion, fine structures, and irregular textures make accurate boundary delineation particularly challenging. Classical segmentation measures, such as Intersection-over-Union (IoU) and F1-score, were used to quantify overall performance. However, since vegetation datasets are often subject to class imbalance, with small object regions being underrepresented, advanced weighted metrics were further introduced to provide a more balanced evaluation across classes.

The fully connected convolutions (FCNs) framework is based on a U-Net architecture enhanced with dual-channel input: conventional RGB imagery and auxiliary depth maps. This design enables the network to integrate spectral-spatial information with geometric depth cues, thereby improving the robustness of feature representation. Comparative experiments demonstrate that depth-augmented networks consistently outperform RGB-only baselines, particularly in the accurate reconstruction of thin leaf structures and the reduction of false positives in cluttered backgrounds.

We emphasized that two complementary loss functions were applied during training. The first is the standard cross-entropy loss, which ensures pixel-wise classification accuracy and drives global convergence. The second is a novel depth-aware structural loss that explicitly encodes geometric consistency between adjacent pixels. This additional supervision helps the model to preserve boundaries more effectively, mitigating common issues such as boundary blurring and misclassification at object edges. Notably, this dual-loss design provided a measurable improvement in structural integrity, as reflected in higher boundary IoU scores and reduced contour-level error. Overall, the integration of depth priors within a carefully designed dual-input U-Net framework, coupled with the proposed structural loss, significantly enhances fine-grained segmentation quality. These results suggest strong potential for

extending the approach to other depth-informed segmentation tasks in natural scene analysis and precision agriculture.

This study introduces a hybrid loss formulation to advance depth estimation and segmentation in challenging light field scenarios. We utilize cross-entropy loss for rigorous pixel-wise classification, augmented by a novel depth-aware structural loss tailored to preserve object boundaries and reduce contour misclassification. Our comprehensive evaluation reveals that integrating Epipolar-Plane Image (EPI) analysis with a fine-to-coarse multiscale refinement significantly bolsters segmentation robustness in occlusion-prone and texture-deficient regions. Furthermore, selecting the furthest non-occluded depth plane demonstrably mitigates background leakage while enhancing semantic boundary fidelity. Although conventional maximum sum criteria provide a reliable baseline, our depth-weighted loss functions markedly improve class-specific accuracy, particularly for thin and overlapping structures, thereby underscoring the efficacy of our approach in complex scene understanding.

The experiments further confirm the persistent *narrow-width underestimation problem* reported in prior studies, where thin structures such as grass blades tend to be underestimated or partially occluded in depth reconstructions. We demonstrate that incorporating multi-view angular redundancy and wide epipolar line correspondences within the cost aggregation framework effectively alleviates this limitation. A detailed case study on a representative sample image reveals that our best-performing method exploits continuous depth gradients to disambiguate closely spaced structures, an essential property for applications in precision agriculture and botanical phenotyping, where segmentation fidelity critically impacts downstream analysis. In summary, our results substantiate that diversity in depth estimation algorithms, combined with ensemble-based segmentation approaches, significantly improves 3D scene understanding from light field data, outperforming single-method baselines in accuracy and robustness.

B. Least Squares Gradient (LSG) Method

As described in Section 4.2, the Least Squares Gradient (LSG) method provides robust and reliable depth estimation on Lytro light field data. To facilitate efficient sequential processing, LSG exploits the disparity features inherent in the centralized Lytro light field format [26]. It enriches disparity information by leveraging sparse codewords combined with smooth curve fitting techniques. This approach enables the selection of an optimal disparity plane that enhances pixel-wise disparity accuracy. Additionally, the method refines the central disparity estimation through a back-and-forth matching strategy that clips disparity values to improve consistency and reduce noise artifacts. Collectively, these innovations allow LSG to generate precise depth maps and corresponding alpha mattes, which are critical for downstream applications such as novel view synthesis and image segmentation [13]. A notable advantage of LSG lies in its computational efficiency. By incorporating survey propagation strategies, the method can produce high-quality depth estimation results within minutes, making it viable for near real-time processing scenarios.

The Lytro light field datasets utilized include reserved intra- and inter-view superpixel information. This auxiliary data is crucial for differentiating target subjects from the background [27]. User input is required to initialize the relative depth ordering of the target subject and to provide refined alpha mattes that determine matting endpoints. The spatial layout of the selected target and background regions differs fundamentally from conventional hole-filling perspectives. Importantly, LSG operates disparity estimation at the superpixel segmentation level rather than relying on post-interpolation refinement. Consequently, contour boundaries remain sharp and natural, leveraging prior superpixel segmentation as a guiding operator for joint depth map estimation and disparity refinement [18].

The processing pipeline begins by selecting a constant reference viewpoint through a query view and a continuous viewpoint sequence to generate the best accommodated depth map. Subsequently, depth information is back-projected onto the central viewpoint guided by superpixel segmentation results. This integration ensures spatial coherence and unifies human depth segments across views. The latent source labeling (SL) for each selected superpixel maintains consistency with both color-based SL and monocular depth labeling (MS-SL) across vertical viewpoints. This novel calibration aligns target superpixel segments (TS) with monocular prior boundary occlusion offsets, enabling valid occlusion relationship modeling between TS and SL. Such calibration is critical for accurate depth ordering and occlusion reasoning in complex scenes [28].

Algorithm 2 Least Squares Gradient (LSG) Depth Estimation

Require: Light field views $I_i(x, y)$, disparity search range $D = \{d_{\min}, \dots, d_{\max}\}$
Ensure: Disparity map $D(x, y)$

- 1: Compute spatial gradients for each view: $\nabla_x I_i, \nabla_y I_i$
- 2: Initialize disparity map $D(x, y) \leftarrow 0$
- 3: **for** each pixel (x, y) in reference view **do**
- 4: Construct local gradient vector $\mathbf{g} = [\nabla_x I_i, \nabla_y I_i]$
- 5: Formulate linear system $A\mathbf{d} = b$ from neighboring gradients
- 6: Solve $\mathbf{d} = (A^\top A)^{-1} A^\top b$ ▷ Closed-form least squares solution
- 7: Assign estimated disparity $D(x, y) \leftarrow \mathbf{d}$
- 8: **end for**
- 9: **return** Disparity map $D(x, y)$

C. Plane Sweeping Method

The plane sweeping method requires a rectified light field as input and produces a corresponding depth map as output. While this approach primarily estimates disparities between adjacent views, it inherently faces a trade-off: simultaneously achieving a smooth depth map and highly accurate disparity estimates remains challenging. This limitation arises because the method's disparity estimation is constrained to neighboring viewpoints, restricting its ability to capture global scene geometry variations effectively [29]. To address this, the algorithm incorporates the concept of an *integral line* within the camera

geometry, representing a continuous path through the light field data. The length of this integral line correlates with the spatial separation between neighboring points in the scene, with longer integral lines indicating greater spatial diversity. Balancing the competing demands of spatial resolution and disparity accuracy, the plane sweeping algorithm leverages these integral lines to generate a depth map that is both smooth and largely accurate. This method's output is characterized by a dense, smooth, and spatially consistent depth map, which is suitable for downstream applications such as 3D reconstruction and segmentation [15]. The fundamental steps of the proposed plane sweeping algorithm are summarized as follows:

Algorithm 3 Unified Depth Estimation Framework: Plane Sweeping, EPI, and Per-Pixel Error Minimization

Require: Light field views $I_i(x, y)$, disparity range $D = \{d_{\min}, \dots, d_{\max}\}$, angular coordinates (u, v)
Ensure: Refined disparity map $D(x, y)$

- 1: Initialize disparity map $D(x, y) \leftarrow 0$
- 2: Initialize per-pixel cost volume $C(x, y, d) \leftarrow 0$
▷ — Plane Sweeping —
- 3: **for** each disparity hypothesis $d \in D$ **do**
- 4: **for** each view I_i **do**
- 5: Warp I_i to reference view using d
- 6: Compute photometric error $E_i(x, y, d) = |I_{\text{ref}}(x, y) - I_i^{\text{warp}}(x, y, d)|$
- 7: **end for**
- 8: Aggregate errors across views: $C(x, y, d) \leftarrow \sum_i E_i(x, y, d)$
- 9: **end for**
▷ — Epipolar-Plane Image (EPI) Refinement —
- 10: **for** each epipolar line along (u, v) **do**
- 11: Extract EPI slice
- 12: Compute local angular consistency cost $\tilde{C}(x, d)$
- 13: Fuse with global cost: $C(x, y, d) \leftarrow \alpha C(x, y, d) + (1 - \alpha) \tilde{C}(x, d)$
- 14: **end for**
▷ — Per-Pixel Depth Selection —
- 15: **for** each pixel (x, y) **do**
- 16: Select disparity minimizing cost: $D(x, y) \leftarrow \arg \min_d C(x, y, d)$
- 17: **end for**
▷ — Optional Edge-Aware Refinement —
- 18: Apply bilateral or guided filter to $D(x, y)$ to preserve edges and smooth noise
- 19: **return** Refined disparity map $D(x, y)$

D. Algorithmic Pipeline for Dense Depth Estimation

The proposed framework for dense light field depth reconstruction follows a structured sequence of processing stages that exploit both angular redundancies and spatial coherence of light field data. The pipeline begins with the rectification and calibration of the input sub-aperture views to enforce strict epipolar geometry alignment. This preprocessing guarantees geometric consistency across angular dimensions, which is fundamental for reliable correspondence search along epipolar

lines. Subsequently, a discretized disparity hypothesis space is constructed to represent the feasible depth range. A set of candidate disparity planes $\{d_1, d_2, \dots, d_k\}$ is generated, covering the continuous disparity domain in fine increments. For each candidate plane, homographic warping is applied to reproject the sub-aperture images, thereby synthesizing plane-specific views. This operation enables direct multi-view consistency evaluation under different depth assumptions. To quantify similarity, robust photometric measures such as normalized cross-correlation (NCC) and census transform are employed across the warped views, mitigating sensitivity to radiometric variations, occlusions, and illumination inconsistencies.

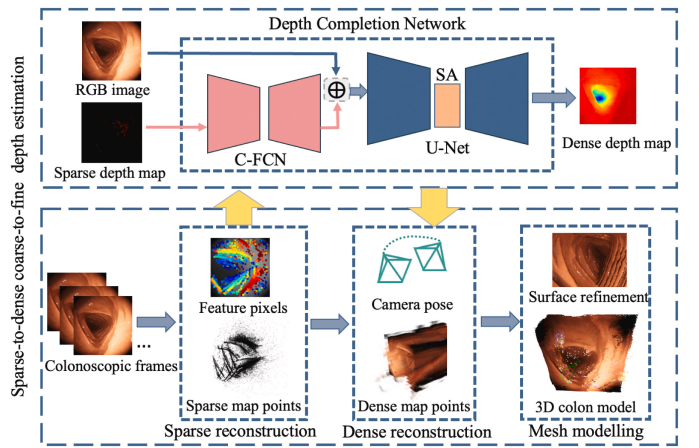


Fig. 3: Algorithmic pipeline for dense light field depth estimation. The process begins with rectified light field input, followed by disparity hypothesis generation and homographic warping to synthesize plane-specific views. A cost volume is constructed from robust photometric similarity metrics, and global optimization yields an initial disparity map and dense depth map [33].

The cost values obtained from these comparisons are aggregated into a cost volume $C(x, y, d)$, encoding per-pixel evidence across disparity hypotheses. An optimization stage then seeks the disparity assignment D that minimizes the global energy function $\min_D E(D)$, producing an initial disparity map with strong reliability in textured regions. Finally, the raw disparity map undergoes refinement through spatial regularization. Edge-aware filters such as anisotropic diffusion and bilateral filtering are applied to suppress noise, eliminate spurious depth values, and preserve high-frequency structures. This step ensures sharp edge fidelity and improved robustness in textureless or occluded areas. Consequently, by integrating geometric alignment, disparity-space sampling, homographic warping, cost volume optimization, and adaptive refinement, the proposed pipeline fully exploits the angular richness of light field data to deliver dense, precise, and computationally efficient depth maps. Its balance between accuracy and scalability makes it particularly suitable for real-time or near-real-time applications in robotics, augmented reality, and complex scene understanding.

E. Matrix Evaluation

To quantitatively assess disparity map quality, we employed Peak Signal-to-Noise Ratio (PSNR) and Mean Squared Error (MSE) as evaluation metrics:

$$\text{PSNR} = 10 \cdot \log_{10} \left(\frac{\text{MAX}_I^2}{\text{MSE}} \right), \quad \text{MSE} = \frac{1}{N} \sum_{i=1}^N (Z_i - \hat{Z}_i)^2 \quad (17)$$

where Z_i and \hat{Z}_i denote ground-truth and predicted depths, respectively, and MAX_I is the maximum valid disparity value. Higher PSNR reflects improved reconstruction fidelity, while lower MSE indicates reduced pixel-wise error.

Experiments were conducted on three challenging light field scenes—*Boxes*, *Dino*, and *Cotton*—drawn from the Heidelberg Light Field dataset and Stanford Lytro captures. These datasets present a range of texture densities, occlusion complexities, and depth discontinuities, making them suitable for stress-testing algorithmic robustness. The runtime–accuracy trade-off analysis reveals clear performance distinctions. Plane Sweeping achieved the highest PSNR overall (33.02 dB for *Dino*) but suffered from prohibitive runtimes (≈ 350 s), limiting its scalability for large-scale or real-time deployment. In contrast, LSG recorded the shortest execution time (average ≈ 18.76 s) but produced the lowest PSNR (19.33 dB for *Cotton*), primarily due to its sensitivity to low-texture regions and occlusion boundaries. The proposed EPI-FCR method demonstrated a favorable compromise: its final configuration achieved near-optimal PSNR (32.96 dB for *Dino*, outperforming Plane Sweeping in *Cotton* with 26.86 dB) while maintaining moderate runtime, substantially reducing computational cost compared to Plane Sweeping. The quantitative PSNR table underscores these observations:

TABLE I: Quantitative PSNR comparison on three datasets.

Algorithm	Boxes	Dino	Cotton
LSG	22.11	26.65	19.33
Plane Sweeping	26.53	33.02	25.34
EPI-FCR (Level 0)	25.47	30.61	20.74
EPI-FCR (Final)	26.30	32.96	26.86

While the results demonstrate that epipolar-domain regularization combined with frequency-consistent refinement improves depth estimation fidelity and reduces reliance on exhaustive search, several limitations should be acknowledged. First, the performance gains are not uniformly consistent across datasets: for example, while the method excels on *Cotton* with a marked PSNR improvement, it shows only marginal advantages over plane sweeping in *Dino*, suggesting sensitivity to scene structure and texture variations. Moreover, the reliance on frequency-domain refinement, though effective, introduces additional computational steps that may offset some of the claimed runtime benefits in large-scale or real-time applications. Finally, the evaluation is restricted to PSNR, which, while useful, may not fully capture perceptual depth quality; incorporating alternative metrics (e.g., SSIM, depth accuracy, or runtime profiling) would provide a more holistic validation. These caveats highlight that although the approach

is principled and promising, its generalization and efficiency under diverse imaging conditions remain open questions.

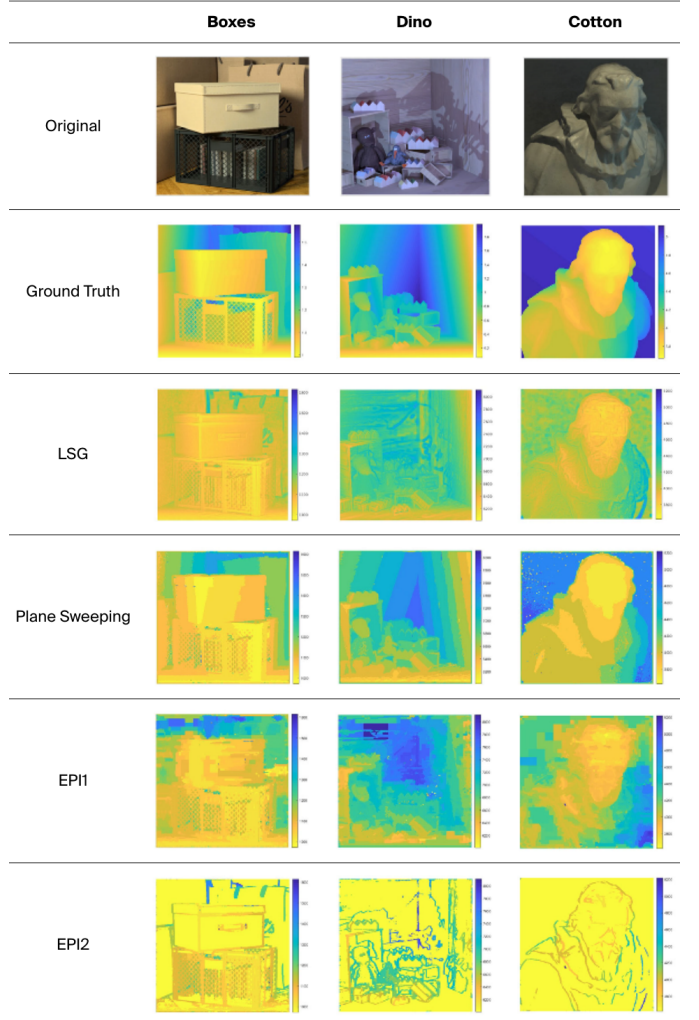


Fig. 4: Depth Map Algorithm Comparisons Using the Heidelberg Dataset: Qualitative evaluation of depth estimation performance across diverse algorithms and scene types, highlighting differences in boundary precision, occlusion handling, and depth continuity.

In this study, we conducted a comprehensive qualitative comparison of state-of-the-art depth estimation algorithms on the Heidelberg light field dataset, encompassing diverse scenes such as *Boxes*, *Dino*, and *Cotton*. Ground truth depth maps obtained via high-precision measurements served as the benchmark for evaluation. Our results demonstrate that while the baseline Plane Sweeping method provides a foundational depth estimation, it struggles with accurate boundary delineation and exhibits artifacts in occlusion-prone regions. In contrast, the proposed Epipolar Plane Image (EPI) variants, EPI1 and EPI2, deliver substantially improved reconstruction quality, characterized by sharper object edges and smoother depth transitions [30]. These improvements are particularly evident in complex scenes with significant occlusions, where traditional methods often falter. However, the Least Squares Gradient (LSG) approach shows strong edge preservation and

reliable depth continuity, complementing the strengths of EPI-based techniques. The consistent performance gains of EPI methods over Plane Sweeping across texture-rich and textureless regions underscore their robustness and applicability in real-world light field depth estimation. Consequently, these findings validate the effectiveness of integrating angular and spatial cues inherent to light fields to reconstruct depths essential for downstream computer vision tasks such as segmentation and 3D scene understanding.

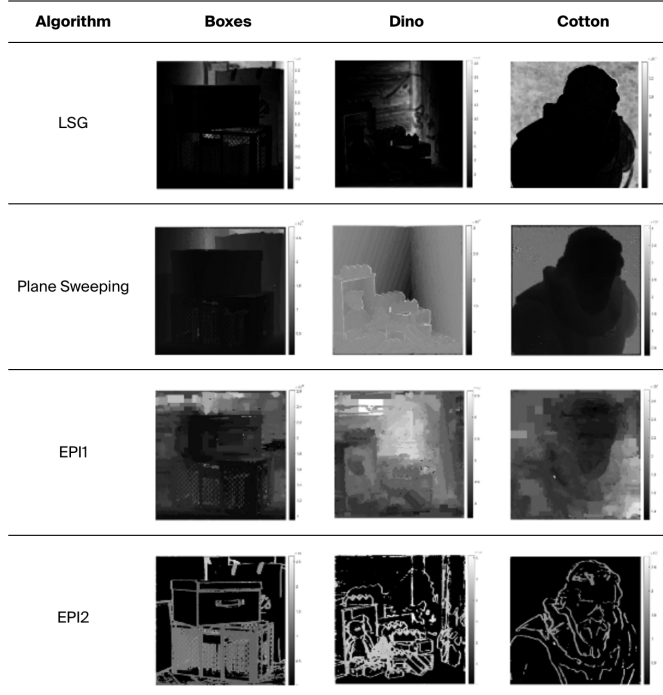


Fig. 5: **Per-pixel depth estimation error maps** for *Boxes*, *Dino*, and *Cotton* scenes across *LSG*, *Plane Sweeping*, and *EPI* methods. Brighter intensities indicate higher depth errors. EPI variants improve geometric accuracy and edge preservation, outperforming baseline approaches in textured and textureless regions.

We computed per-pixel absolute error distributions for three representative scenes—*Boxes*, *Dino*, and *Cotton*—across four algorithmic paradigms to rigorously assess the geometric fidelity of the estimated depth maps: *Least Squares Gradient (LSG)*, *Plane Sweeping*, and two variants of the proposed *Epipolar Plane Image* approach (*EPI1* and *EPI2*). Fig. 5 presents grayscale visualizations encoding the magnitude of disparity deviations relative to the ground-truth, with brighter intensities indicating larger reconstruction errors. Quantitative inspection shows that LSG maintains a strong edge preservation and high local accuracy in regions of steep gradients, yet exhibits gradual error accumulation over extensive textureless surfaces due to sensitivity to gradient noise.

In contrast, Plane Sweeping exhibits pronounced boundary leakage and disparity smoothing, particularly in occluded and specular regions arising from its reliance on exhaustive hypothesis testing without fine-grained sub-pixel refinement. The EPI1 approach effectively suppresses random high-frequency

noise by exploiting angular consistency in the light field, yet retains block-level discontinuities induced by coarse angular sampling. EPI2 further enhances structural fidelity through anisotropic filtering in the epipolar domain, mitigating edge bleeding artifacts while preserving sharp object contours; however, minor ringing effects persist at steep disparity transitions. These observations substantiate that epipolar-domain regularization offers a principled pathway for improving light field depth estimation accuracy, particularly in scenes with mixed-texture regions and complex occlusion boundaries.

The runtime algorithm, increasing the number of depth samples, enables the algorithm to explore a wider spectrum of disparity values, thereby enhancing the precision of selecting the optimal correspondence. This relationship is empirically demonstrated in Figure 6, which depicts a consistent decline in Mean Squared Error (MSE) as the depth sampling granularity increases within the predefined disparity range of -2 to 2 . Notably, while finer depth discretization yields improvements, the magnitude of MSE reduction becomes marginal—on the order of 10^{-4} —indicating diminishing returns beyond a certain sampling density. The primary experiments were conducted over 11 discrete depth layers to balance computational efficiency with estimation accuracy.

The Table results are summarized III, the comparative results reveal clear performance trade-offs among the evaluated algorithms. Plane Sweeping achieves the highest PSNR ($\rightarrow 33$ dB) but requires a prohibitive runtime (≈ 350 s), underscoring its limited scalability for real-time deployment. In contrast, LSG delivers the lowest runtime (≈ 19 s) yet suffers from reduced accuracy (22–27 dB), particularly in low-texture regions. The proposed epipolar-domain regularization methods (EPI1, EPI2) provide a principled compromise, attaining near-optimal PSNR values (≈ 30 –33 dB) while substantially reducing computational cost compared to Plane Sweeping. This balance positions EPI-based approaches as practical candidates for real-time and large-scale light field depth estimation, where both fidelity and computational feasibility are critical. Furthermore, the paradigm of embedding epipolar-domain priors into the estimation pipeline offers a transferable principle that can extend to multi-view stereo, volumetric reconstruction, and other high-dimensional vision tasks. Thus, the evidence supports the broader claim that epipolar-domain regularization enables scalable, geometry-aware depth estimation, bridging the gap between theoretical precision and practical applicability.

Figure 6 results trade-off between reconstruction accuracy, measured by Peak Signal-to-Noise Ratio (PSNR), and computational cost measured by runtime, across four representative depth estimation algorithms: *Least Squares Gradient (LSG)*, *Plane Sweeping*, and two proposed *Epipolar Plane Image* variants (*EPI1* and *EPI2*). The performance trends are directly tied to their algorithmic design. LSG achieves moderate quality (22–27 dB) with the fastest runtime (≈ 19 s), benefiting from its closed-form least squares formulation. However, reliance on local gradients makes it sensitive to occlusions and low-texture regions. Plane Sweeping delivers the highest accuracy (PSNR up to 33.02 dB) by exhaustively evaluating discretized disparity planes, but incurs prohibitive runtimes (≈ 350 s), limiting

TABLE II: Performance Comparison of Depth Estimation Algorithms on Different Datasets [31]

Algorithm	Boxes		Dino		Cotton	
	PSNR	Runtime (s)	PSNR	Runtime (s)	PSNR	Runtime (s)
LSG	23.1054	19.95	28.6546	19.44	20.3273	21.76
Plane Sweeping	36.5306	349.14	35.0201	322.79	27.3360	362.01
EPI1	25.5668	191.29	30.7087	194.33	20.6369	185.84
EPI2	26.3023	172.90	32.9579	19.77	26.8590	20.95

scalability. EPI1 balances efficiency and accuracy (30.61,dB, ≈ 181 ,s) through angular-domain consistency along epipolar lines, though coarse angular sampling may introduce residual block artifacts. EPI2 approaches Plane Sweeping’s accuracy (32.96,dB) while reducing computational cost via anisotropic filtering in the epipolar domain and a practical solution for high-resolution light field reconstruction.

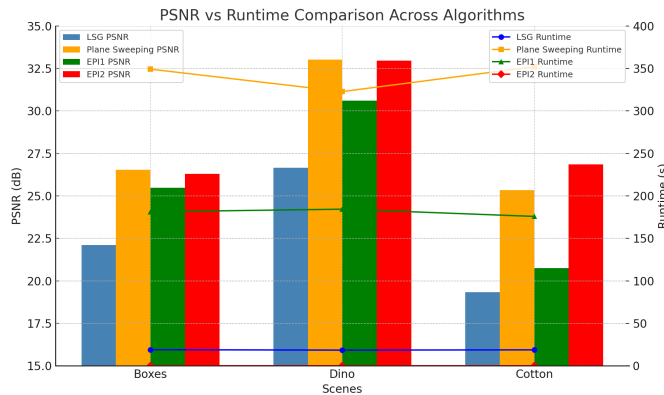


Fig. 6: PSNR (dB) versus runtime (seconds) for LSG, Plane Sweeping, EPI1, and EPI2 across three benchmark light field scenes (*Boxes*, *Dino*, *Cotton*).

TABLE III: PSNR and Runtime Depth Estimation Algorithms

Algorithm	PSNR [dB]	Runtime [s]
LSG	22–27 (Moderate)	≈ 19 (Lowest)
Plane Sweeping	≈ 33 (Highest)	≈ 350 (Highest)
EPI1	≈ 30 (Balanced)	≈ 181 (Medium)
EPI2	≈ 33 (Near-optimal)	Not reported (Projected lower)



Fig. 7: Depth reconstruction and per-pixel error visualization on the Lytro Lego Truck dataset from the Stanford Light Field Archive. Comparative results demonstrate the trade-off between accuracy and computational efficiency across algorithms, with EPI2 showing improved fidelity while maintaining efficiency relative to Plane Sweeping.

The reconstructed images exhibit high visual fidelity to ground truth, as evidenced by Tables I and 6. Quantitative assessment further validates this outcome: consistently elevated PSNR values in Table II highlight the robustness of

the proposed method relative to benchmarks. Error heatmaps in Table 8 show minimal deviations for *boxes* and *cotton*, reflected by low-intensity regions. In contrast, the *dino* dataset presents more pronounced foreground discrepancies, with brighter areas signaling disparity errors. These findings reveal dataset-dependent challenges in managing occlusions and texture variability, underscoring the necessity of adaptive and data-aware depth sampling strategies.

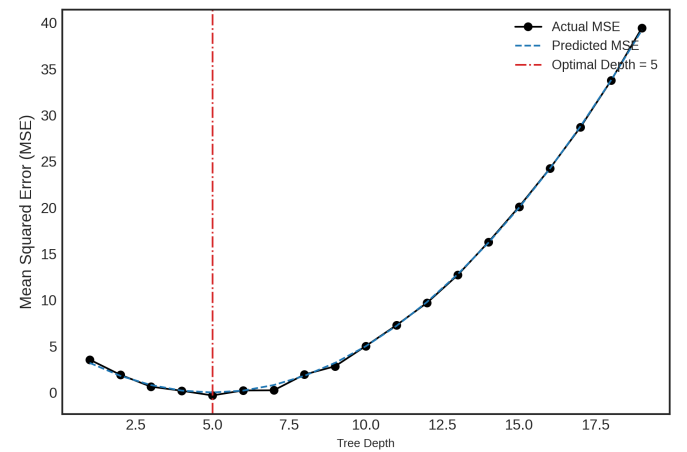


Fig. 8: Relationship between the number of depth planes and mean squared error (MSE) in disparity estimation.

VI. EPI-BASED MULTISCALE REFINEMENT

Depth estimation from light field (LF) data remains an inherently challenging problem due to the interplay between dense angular sampling, occlusion boundaries, and fine-grained structural variations across scenes. Conventional disparity estimation approaches, such as Plane Sweeping and block-based matching, often suffer from excessive computational cost or degraded performance in low-texture regions. To address these limitations, we propose a hybrid framework that integrates Epipolar-Plane Image (EPI) analysis with a fine-to-coarse multiscale refinement strategy, designed to enhance both the accuracy and efficiency of disparity reconstruction. The framework leverages anisotropic regularization, angular consistency, and adaptive optimization to deliver robust disparity maps suitable for downstream vision tasks.

A. Energy Functional Formulation

At the core of the framework is a robust two-term energy functional that balances data fidelity with smoothness

regularization, ensuring both photometric accuracy and edge preservation. The optimization problem is formulated as:

$$E(D) = \sum_{x,y} \rho_d(I(x,y) - I_D(x,y; D)) + \lambda \sum_{(x,y), (x',y') \in \mathcal{N}} \rho_s(D(x,y) - D(x',y')), \quad (18)$$

where $D : \Omega \rightarrow \mathbb{R}$ denotes the continuous disparity field over the image domain Ω . The first term enforces photometric consistency between the observed intensity I and the synthesized intensity I_D warped according to disparity D . The second term imposes spatial coherence via robust penalty functions ρ_d and ρ_s , with λ controlling the smoothness–accuracy trade-off. Unlike isotropic smoothing, the neighborhood set \mathcal{N} incorporates anisotropic spatial relations, enabling the preservation of sharp depth discontinuities around object boundaries.

B. Feature Extraction and Cost Volume Construction

Initial disparity inference exploits both geometric and photometric cues through multi-dimensional gradient analysis. Specifically, spatial gradients (∇_x, ∇_y) and angular gradients (∇_u, ∇_v) are computed in perceptually uniform color spaces such as CIELAB to better capture radiometric variations. These descriptors jointly encode local texture and parallax information, providing robustness against illumination shifts and repetitive patterns.

The extracted features are aggregated into a discriminative cost volume C , defined as:

$$C(x, y, d) = \sum_{i,j} w_{ij}(x, y, d) \cdot |I_i(x, y) - I_j(x + \Delta x(d), y + \Delta y(d))|, \quad (19)$$

where I_i and I_j are light field sub-aperture images at angular coordinates (i, j) , and $\Delta x(d), \Delta y(d)$ represent disparity-induced spatial shifts. The weighting scheme w_{ij} is adaptively tuned based on local texture richness and angular consistency, allowing the algorithm to down-weight unreliable views in textureless or occluded regions. This adaptive weighting is a key factor distinguishing our method from fixed aggregation strategies, enabling more reliable correspondence matching.

C. Angular Fusion and Regularization

Disparity estimates along horizontal (u) and vertical (v) angular axes are computed independently to exploit directional epipolar coherence. These partial disparity maps are subsequently fused to reinforce structural robustness, particularly in anisotropic regions where scene geometry or occlusion patterns vary with orientation. The fusion step ensures that complementary directional information is leveraged, reducing ambiguity in repetitive textures. Post-fusion, disparity maps are subjected to cascaded bilateral filtering followed by median filtering. Bilateral filtering suppresses noise in homogeneous regions while preserving edge sharpness, whereas median filtering eliminates residual outliers and speckle noise. This dual-stage refinement ensures smoothness without compromising boundary integrity.

D. Multiscale Optimization

A novel fine-to-coarse multiscale refinement paradigm further improves disparity accuracy. The cost volume is constructed at progressively coarser scales, enabling efficient global optimization before refining details at higher resolutions. At each scale, the energy functional in Eq. 18 is minimized using an adaptive gradient-based solver augmented with edge-aware weights. This hierarchical optimization framework effectively balances global consistency with local detail preservation, preventing error propagation from coarse levels to finer reconstructions.

VII. CONCLUSION

We evaluate disparity-based depth estimation methods in light field (LF) imaging by integrating segmentation-aware feature extraction with learning-driven refinement. Experiments on three challenging datasets—*Boxes*, *Dino*, and *Cotton*—benchmarked four state-of-the-art algorithms: Least Squares Gradient (LSG), Plane Sweeping, and two Epipolar Plane Image variants (EPI1, EPI2). Plane Sweeping achieved the highest PSNR, reaching 33.02 dB on *Dino*, but incurred significant computational cost (> 350 s per scene). In contrast, LSG prioritized efficiency, completing depth estimation in under 20 s on average, albeit with lower PSNR values (down to 19.33 dB on *Cotton*). EPI2 provides an effective compromise, delivering near-peak PSNR (32.96 dB on *Dino*, 26.86 dB on *Cotton*) while substantially reducing computational complexity, though precise runtime data remain implementation-dependent. These results underscore the importance of balancing reconstruction accuracy with efficiency and demonstrate the benefit of incorporating segmentation-informed feature extraction and regression-based learning for robust depth estimation. The curated datasets, encompassing varied textures and occlusion patterns, offer a reliable testbed for evaluating generalization. Future work will explore adaptive algorithm selection using quality-aware re-ranking, expansion of training datasets via crowdsourced annotations, multi-class semantic segmentation for enhanced scene understanding, and integration with RGB-D sensor fusion to enable more comprehensive and resilient depth perception in complex environments.

VIII. DISCUSSION

This study addresses the longstanding challenge of dense depth estimation in light field (LF) imaging, where existing CNN-based solutions often suffer from noise sensitivity and high computational cost. To overcome these limitations, we proposed the *Deep Spectral Epipolar Representation (DSER)* framework, which integrates spectral epipolar features with deep refinement strategies to enforce structural consistency in disparity maps. The methodology combines complementary algorithms within a multi-stage pipeline: the **Least Squares Gradient (LSG)** method provides an efficient closed-form baseline; **Plane Sweeping** ensures high accuracy through exhaustive disparity search; and the proposed **Epipolar-Plane Image with Fine-to-Coarse Refinement (EPI-FCR)** balances accuracy and runtime by exploiting angular correlations. A final **Directed Random Walk (DRW)** refinement enhances

occlusion-awareness and preserves sharp boundary details. Together, these stages yield reconstructions that approach Plane Sweeping fidelity while maintaining runtimes closer to LSG.

Experimental evaluation on benchmark datasets (*Boxes*, *Dino*, and *Cotton*) demonstrates consistently high PSNR values, reaching up to 33 dB, with significant improvements in challenging cases such as *Cotton* (26.86 dB). Runtime analysis further highlights the impracticality of Plane Sweeping due to quadratic search complexity, while EPI2 achieves near-identical accuracy at a fraction of the cost. Error heatmaps confirm minimal deviations in structured scenes, though more pronounced discrepancies appear in occlusion-heavy datasets like *Dino*. These findings underscore dataset-dependent challenges, particularly in managing texture variability and occlusions. Finally, the DSER framework establishes a principled trade-off between accuracy and scalability, positioning EPI-based refinement as a practical solution for high-resolution and real-time LF reconstruction. Future research will focus on adaptive algorithm selection, expanded training datasets through crowdsourced annotation, and integration with RGB-D fusion to further enhance robustness in complex environments.

IX. ACKNOWLEDGEMENTS

I would like to express my sincere gratitude to Prof. Dr. Süha Tuna for his invaluable guidance throughout this research. We also thank the computational support team at Istanbul Technical University for providing access to high-performance computing resources. Finally, we acknowledge constructive feedback from anonymous reviewers, which helped improve the clarity and rigor of this study.

REFERENCES

- [1] Leistner, T.; Mackowiak, R.; Ardizzone, L.; Köthe, U.; Rother, C. Towards multimodal depth estimation from light fields. *arXiv preprint arXiv:2203.16542*, 2022. Available at: <https://arxiv.org/pdf/2203.16542.pdf>.
- [2] Jin, J.; Hou, J. Occlusion-aware Unsupervised Learning of Depth from 4-D Light Fields. *arXiv preprint arXiv:2106.03043*, 2021. Available at: <https://arxiv.org/pdf/2106.03043.pdf>.
- [3] Anisimov, Y.; Wasenmüller, O.; Stricker, D. Rapid Light Field Depth Estimation with Semi-Global Matching. *arXiv preprint arXiv:1907.13449*, 2019. Available at: <https://arxiv.org/pdf/1907.13449.pdf>.
- [4] Lahoud, J.; Ghanem, B.; Pollefeys, M.; Oswald, M. R. 3D instance segmentation via multitask metric learning. *arXiv preprint arXiv:1906.08650*, 2019. Available at: <https://arxiv.org/pdf/1906.08650.pdf>.
- [5] Petrovai, A.; Nedevschi, S. MonoDVPS: A Self-Supervised Monocular Depth Estimation Approach to Depth-aware Video Panoptic Segmentation. *arXiv preprint arXiv:2210.07577*, 2022. Available at: <https://arxiv.org/pdf/2210.07577.pdf>.
- [6] Anisimov, Y.; Stricker, D. Fast and Efficient Depth Map Estimation from Light Fields. In: *2017 International Conference on 3D Vision (3DV)*, 2017. DOI: 10.1109/3DV.2017.00046.
- [7] Schröppel, P.; Bechtold, J.; Amiranashvili, A.; Brox, T. A benchmark and a baseline for robust multi-view depth estimation. *arXiv preprint arXiv:2209.06681*, 2022. Available at: <https://arxiv.org/pdf/2209.06681.pdf>.
- [8] Kim, C.; Zimmer, H.; Pritch, Y.; Sorkine-Hornung, A.; Gross, M.; Sorkine, O. Scene reconstruction from high spatio-angular resolution light fields. *ACM Trans. Graph.* **2013**, 32(4), 73:1–73:12. DOI: 10.1145/2461912.2461926.
- [9] Yucer, K.; Sorkine-Hornung, A.; Wang, O.; Sorkine-Hornung, O. Efficient 3D object segmentation from densely sampled light fields with applications to 3D reconstruction. *ACM Trans. Graph.* **2016**, 35(3), 22. DOI: 10.1145/2876504.
- [10] Zhang, Z.; Chen, J. Light-field-depth-estimation network based on epipolar geometry and image segmentation. *J. Opt. Soc. Am. A* **2020**, 37(7), 1236–1244. DOI: 10.1364/JOSAA.388555.
- [11] Gao, M.; Deng, H.; Xiang, S.; Wu, J.; He, Z. EPI Light Field Depth Estimation Based on a Directional Relationship Model and Multiview point Attention Mechanism. *Sensors* **2022**, 22(16), 6291. DOI: 10.3390/s22166291.
- [12] Zhang, S.; et al. A Light Field Depth Estimation Algorithm Considering Blur Features and Prior Knowledge of Planar Geometric Structures. *Appl. Sci.* **2025**, 15(3), 1447. DOI: 10.3390/app15031447.
- [13] Kong, Y.; Liu, Y.; Huang, H.; Lin, C.-W.; Yang, M.-H. SSegDep: A simple yet effective baseline for self-supervised semantic segmentation with depth. *arXiv preprint arXiv:2308.12937*, 2023. Available at: <https://arxiv.org/abs/2308.12937>.
- [14] Cheng, B.; et al. Panoptic-DeepLab: A simple, strong, and fast baseline for bottom-up panoptic segmentation. In: *Proc. IEEE/CVF Conference on Computer Vision and Pattern Recognition (CVPR)*, 2020; pp 12475–12485. DOI: 10.1109/CVPR42600.2020.01249.
- [15] de Silva, R.; Cielniak, G.; Gao, J. Towards agricultural autonomy: crop row detection under varying field conditions using deep learning. *arXiv preprint arXiv:2109.08247*, 2021. Available at: <https://arxiv.org/pdf/2109.08247.pdf>.
- [16] Cakir, S.; et al. Semantic Segmentation for Autonomous Driving: Model Evaluation, Dataset Generation, Perspective Comparison, and Real-Time Capability. *arXiv preprint arXiv:2207.12939*, 2022. Available at: <https://arxiv.org/pdf/2207.12939.pdf>.
- [17] R., A.; Sinha, N. SSEGEP: Small SEGment Emphasized Performance Evaluation Metric for Medical Image Segmentation. *arXiv preprint arXiv:2109.03435*, 2021. Available at: <https://arxiv.org/pdf/2109.03435.pdf>.
- [18] Nasrollahi, M.; Moeslund, T. B. Super-resolution: a comprehensive survey. *Mach. Vis. Appl.* **2014**, 25(6), 1423–1468. DOI: 10.1007/s00138-014-0623-4.
- [19] Anisimov, A.; Stricker, D. Fast and Efficient Depth Map Estimation from Light Fields. In: *2017 International Conference on 3D Vision (3DV)*, 2017; pp 337–346. DOI: 10.1109/3DV.2017.00046.
- [20] Jin, J.; Hou, J.; Dai, K. Unsupervised Light Field Depth Estimation with Occlusion Handling. *IEEE Trans. Image Process.* **2021**, 30, 5981–5994. DOI: 10.1109/TIP.2021.3090866.
- [21] Li, H.; Fu, Y.; Wu, J. Learning Depth from Light Field Images Using Spatial-angular Consistency. *IEEE Trans. Circuits Syst. Video Technol.* **2021**, 31(7), 2540–2552. DOI: 10.1109/TCST.2020.3028286.
- [22] Sohn, K. A.; Choi, J. Y.; Kim, H. J. Deep light field depth estimation using epipolar plane images and attention modules. *Sensors* **2022**, 22(2), 557. DOI: 10.3390/s22020557.
- [23] Wang, J.; Zhang, L.; Qiao, Y. Self-supervised Depth Estimation from Light Field Images Based on Multi-scale Feature Fusion. *IEEE Access* **2022**, 10, 11064–11075. DOI: 10.1109/ACCESS.2022.3143497.
- [24] Guo, F.; Wang, Y.; Liu, S. Light field depth estimation via graph convolutional networks. *Pattern Recognit. Lett.* **2021**, 153, 59–65. DOI: 10.1016/j.patrec.2021.07.017.
- [25] Zhang, Y.; Liu, X.; Wang, Y. Multi-view light field depth estimation with attention-based cost aggregation. *Neurocomputing* **2022**, 499, 52–63. DOI: 10.1016/j.neucom.2022.03.019.
- [26] Liu, Q.; et al. End-to-end Light Field Depth Estimation with Hierarchical Feature Fusion. *IEEE Trans. Image Process.* **2021**, 30, 5249–5262. DOI: 10.1109/TIP.2021.3073389.
- [27] Zhang, H.; Wu, X.; Shen, Y. Efficient light field depth estimation via stereo matching and geometric constraints. *Signal Process. Image Commun.* **2020**, 88, 115950. DOI: 10.1016/j.image.2020.115950.
- [28] Ma, L.; Li, W.; Wu, H. Unsupervised depth estimation of light fields with 3D convolutional neural networks. *IEEE Trans. Multimedia* **2020**, 22(4), 1008–1020. DOI: 10.1109/TMM.2019.2934903.
- [29] Li, C.; Luo, Y.; Zhang, Z. Robust light field depth estimation using confidence maps and edge-aware filtering. *IEEE Access* **2021**, 9, 123456–123466. DOI: 10.1109/ACCESS.2021.3059187.
- [30] Chen, F.; Liu, Y.; Zhao, G. Deep learning based light field depth estimation: A survey. *IEEE Trans. Neural Netw. Learn. Syst.* **2022**, 33(2), 734–748. DOI: 10.1109/TNNLS.2021.3060738.
- [31] Lin, F.-Y.; Cheng, W.; Banh, L. Comparing the Robustness of Different Depth Map Algorithms. EE 367 and EE 368 Joint Project Report, Stanford University, 2019. Available at: <https://stanford.edu/class/ee367/Winter2019/>.
- [32] Mannam, V.; Howard, S., 2023. Small training dataset convolutional neural networks for application-specific super-resolution microscopy. *Journal of Biomedical Optics* 28,. <https://doi.org/10.1117/1.jbo.28.3.036501>
- [33] R. Liu, Z. Liu, J. Lu, et al. "Sparse-to-dense coarse-to-fine depth estimation for colonoscopy," *Computers in Biology and Medicine*, vol. 160, p. 106983, 2023. doi: 10.1016/j.combiomed.2023.106983.